Tidal grounding-line migration modulated by subglacial hydrology

K. L. P. Warburton[1], D. R. Hewitt[2], and J. A. Neufeld[1,3,4]

[1]Institute of Theoretical Geophysics, Department of Applied Mathematics and Theoretical Physics, University of Cambridge, Wilberforce Road, Cambridge CB3 0WA, UK
[2]Department of Mathematics, University College London, 25 Gordon Street, London, WC1H 0AY, UK
[3]BP Institute, University of Cambridge, Madingley Rise, Cambridge CB3 0EZ, UK
[4]Department of Earth Sciences, Bullard Laboratories, University of Cambridge, Madingley Rise, Cambridge CB3 0EZ, UK

Key Points:

- Hydraulic resistance of the subglacial environment limits the speed of grounding-line migration
- Speed of grounding-line migration may differ between incoming and outgoing tides
- Asymmetric response of the grounding zone can act as a non-linear filter on the tidal forcing

Corresponding author: Katarzyna Warburton, `klpw3@cam.ac.uk`

Abstract

We present a mathematical model of the hydrology of grounding-line migration on tidal timescales, in which the ice acts elastically, overlying a connected hydrological network, with the ocean tides modelled by an oscillating far-field fluid height. The upstream grounding-line migration is driven by a fluid pressure gradient through the grounding zone, while the downstream migration is limited by fluid drainage through the till. The two processes are described using separate travelling-wave solutions, based on a model of fluid flow under an elastic sheet. The asymmetry between the up- and downstream motion allows the grounding line to act as a non-linear filter on the tidal forcing as the pressure signal propagates upstream, and this frequency modulation is discussed in the context of velocity data from ice streams across Antarctica to provide a novel constraint on till permeability.

Plain Language Summary

The grounding zone, where the ice sheet transitions from contact with the bed to floating on the ocean, plays an important role in understanding the contribution of polar ice sheets to sea level rise. This model explores how ocean water can be pumped through the grounding zone to the region underneath ice sheets as the ocean tides go in and out. Water present underneath ice sheets can make the ice flow faster. We show that the difference between how quickly the water flows into and out of the grounding zone could explain some observations of tidal variations in glacier speed, and raises questions for the amount of melting happening underneath ice sheets.

1 Introduction

The grounding zone of an ice sheet represents the region over which the ice ceases to be supported by the bed and forms an ice shelf floating over the ocean. Understanding grounding-line migration is of key importance in models of glacial dynamics and global climate. Ice that has passed the grounding line contributes to global sea level rise and so must be considered lost in mass balance calculations (Bamber & Rivera, 2007; Shepherd et al., 2012), while the incursion of ocean water at the grounding line enhances melting from the base of ice shelves, decreasing the buttressing of grounded ice (Jenkins et al., 2010). Further, the grounding zone represents a transition region where the ice lifts up from its base and the basal traction dramatically decreases (Gillet-Chaulet & Durand, 2010), so assessing the stability of marine ice sheets relies on determining the grounding-line position relative to topographic pinning points (Schoof, 2007; Gudmundsson, 2013).

Grounding lines are not static but migrate on hourly to multi-annual timescales. Over the daily tidal cycle, grounding lines move back and forth across grounding zones that can be several kilometres wide (Rignot et al., 2011; Bamber et al., 2009). Ice has a visco-elastic rheology, so that over timescales longer than the Maxwell time, the response of the ice is mainly viscous, while on hourly to daily timescales, the response of the ice is predominantly elastic (Holdsworth, 1969; Larour et al., 2005), as illustrated by flexural patterns observed close to the grounding line (Brunt et al., 2010; Vaughan, 1995). For example, detailed measurements on the Rutford Ice Stream reveal a flexural wave propagating across the grounding zone over the tidal cycle, characteristic of this elastic behaviour (Minchew et al., 2017).

Recent observations have shown that tides can affect glacial dynamics far upstream of the grounding zone. Tidal modulations of surface velocities have been observed in ice shelves and sheets across Antarctica and Greenland (Padman et al., 2018). Ocean tides are composed of diurnal and semidiurnal components. While some glaciers, such as the Bindschadler Ice Stream (Anandakrishnan et al., 2003) and the Whillans Ice Stream (Bindschadler et al., 2003) respond at the same frequency as the tidal forcing, other locations,

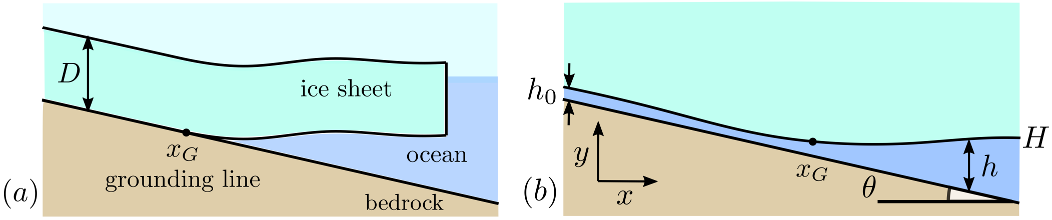

Figure 1. (a) A schematic showing an elastic ice sheet floating on the ocean, lifting off from the bed at the grounding line. (b) Close-up of the region near the grounding line showing the notation of the model.

such as the Rutford Ice Stream (Gudmundsson, 2006; Minchew et al., 2017) and Beardmore Glacier (Marsh et al., 2013), exhibit velocity variations at the fortnightly frequency of the apparent 'beat' between the true tidal components. To generate a 14-day frequency in the surface velocity from daily tides requires a non-linear mechanism to act between the tidal forcing and velocity response (Rosier et al., 2015).

The origin of this non-linear response of the surface velocity remains enigmatic. Previous authors have suggested that the tidal response is modulated by the impact of the visco-elastic rheology on extensional stresses within the ice (Rosier & Gudmundsson, 2018), or by a highly non-linear basal drag law (Rosier et al., 2015). The traction at the base of an ice sheet is strongly dependent on the water pressure there (Tulaczyk et al., 2000; Iverson, 2010). Rosier & Gudmundsson (2020) demonstrated that tidal variations in basal traction at the grounding line are a dominant factor in determining the large scale velocity of marine ice sheets, suggesting the need to accurately assess lubrication by subglacial water across the grounding zone.

Here we explore the response of the grounding zone to ocean tidal forcing, by focussing on the dynamics of water transport through the grounding zone over the tidal cycle. Previous models of tidal grounding-line migration have neglected the hydrodynamics of the subglacial environment. Sayag & Worster (2013) found the equilibrium grounding-line position for a uniform elastic ice sheet at a given ocean height. Tsai & Gudmundsson (2015) considered the impact of variable ice thickness on the static equilibrium position of the grounding line, and proposed a fracture-mechanics model for the incoming tide. Walker et al. (2013) suggested that glaciers could periodically 'gulp' ocean water as the tide comes in. In this paper, we more closely examine the forces driving flow in the subglacial cavity. We find that the asymmetry between the fast advance of the incoming tide and the slow drainage during the outgoing tide produces an asymmetry in grounding zone dynamics over the tidal cycle. By studying the dynamics of water transport across the grounding line over the tidal cycle we describe a self-consistent mechanism coupling the grounding-line migration and subglacial hydrology.

2 The model

We model the influence of subglacial hydrology on tidally-induced grounding-line motion by considering a flow line ice sheet of uniform depth D resting on a bed sloping upwards inland at an angle θ (see figure 1). The base of the ice is at $y = H(x,t)$, and the depth of the subglacial cavity is $h(x,t) = H+\theta x$ (figure 1). Upslope of the grounding line, between the bed and the base of the ice, we parametrise a distributed subglacial hydrological network by an effective water film of thickness h_0, with a hydraulic transmissivity proportional to h_0^3 (e.g. Le Brocq et al., 2009; Bougamont et al., 2014). Far upslope of the grounding line, $h \to h_0$ as $x \to -\infty$, while over the ocean the ice sheet is in isostatic balance, moving up and down with the ocean tides so $H(x,t) \to H_o(t)$ as $x \to \infty$. Since the depth of the cavity transitions smoothly to the effective depth of the subglacial film, we arbitrarily define the grounding line to be the furthest upstream point at which the water depth is above a threshold value, $h(x_G(t),t) = 1.5h_0$.

We note that the role of the bedslope angle θ is to set a hydraulic gradient in the subglacial environment, and therefore can also represent the effect of a gradient in ice thickness across the grounding zone. With this interpretation, the setup can also describe the dynamics of grounding zones on retrograde slopes under a thinning ice sheet, where θ takes the value of $\theta - \rho_i/\rho_w \frac{dD}{dx}$ (see supporting information). In this case, we use the average value of D to evaluate the bending stiffness. Similarly, θ and h_0 may be slowly varying across the grounding zone without qualitatively affecting the results, but for simplicity we take representative, constant values.

In this paper we seek to quantify the ocean water present in the grounding zone to understand the tidal variations in basal drag on the ice above. We first consider the response of the grounding zone to idealised tides that fall or rise with constant speed, and then consider the response to more realistic tides with both solar and lunar components. Having developed a theory to account for general tidal speeds, we then force the grounding-line model with the full spectrum of tidal components.

2.1 The elastic response of the ice

On the timescale of daily tides, ice behaves predominantly elastically Vaughan (1995). For simplicity, we consider a constant ice thickness D across the grounding zone. Tidal fluctuations in height are small relative to the thickness, and hence we model the ice sheet as an elastic beam of bending stiffness $B = ED^3/12(1-\nu^2)$, with Young's modulus $E = 0.32 - 3.9$GPa and Poisson ratio $\nu = 0.3$ (Vaughan, 1995). Spatial variations in the profile of the ice $H(x,t)$ thus exert a bending stress (pressure) $B\frac{\partial^4 H}{\partial x^4}$ on the water below.

Where the ice is floating, a force balance between hydrostatic pressure and bending stresses implies that the static profile of the ice is governed by

$$\frac{\partial}{\partial x}\left(\rho g H + B\frac{\partial^4 H}{\partial x^4}\right) = 0, \tag{1}$$

where ρ is the density of water and g the gravitational acceleration. Over the ocean, the ice becomes flat, and its height is set by a hydrostatic balance with the far-field ocean height. Upstream of the grounding line, the ice rests on its bed. These constraints provide enough conditions to determine the static position of the grounding line as a function of the ocean height, as considered by Sayag & Worster (2011) (see also supporting information). The dynamic response of the grounding line when the ocean height varies over tidal timescales, however, requires coupling of the ice dynamics to the motion of ocean water driven in and out of the subglacial cavity by the motion of the ice.

2.2 The dynamics of the water

For moderate bedslope at the grounding line, the subglacial cavity is much longer than it is deep, so tidally-driven flows are mainly horizontal. In this geometry the pressure within the cavity is given approximately by

$$p = \rho g(H-y) + B\frac{\partial^4 H}{\partial x^4}. \tag{2}$$

Elastic and hydrostatic pressure gradients across the subglacial cavity drive a water flux through the subglacial system, resisted by drag in the hydraulic network. For simplicity, and in keeping with previous studies (Le Brocq et al., 2009; Bougamont et al., 2014), we model the conductivity of the distributed system by a laminar flow law, such that the flux through a layer of depth h is given by

$$q = -\frac{h^3}{12\mu}\frac{\partial p}{\partial x}, \tag{3}$$

where μ is the viscosity of water. Conservation of water across the grounding zone requires that

$$\frac{\partial h}{\partial t} = -\frac{\partial q}{\partial x} = \frac{\partial}{\partial x}\left[\frac{\rho g}{12\mu}h^3\left(\frac{\partial H}{\partial x} + \frac{B}{\rho g}\frac{\partial^5 H}{\partial x^5}\right)\right]. \tag{4}$$

As the ocean height varies over the tidal cycle, $H(x,t) \to H_o(t)$ as $x \to \infty$, $h(x,t) \to h_0$ as $x \to -\infty$, and the hydrology of the grounding zone evolves according to (4).

3 Results and Discussion

We proceed to highlight the asymmetry between incoming and outgoing tides by first considering each case separately. The resultant reduced model is then used to understand the non-linear response of the grounding zone to oscillatory tidal forcing.

3.1 Response of the grounding zone to the rising tide

We first consider the effect of the rising tide on the subglacial system, considering a constant tidal speed. Numerical solutions of the ice-water response from integration of equation (4) are shown in figure 2a, initialised in the static equilibrium elastic position (Sayag & Worster, 2011).

For a steadily rising tide, the ice sheet quickly settles to a steady travelling-wave solution that migrates inland at the speed of the rising tide, with a series of flexural waves propagating through the grounding zone (figure 2a). As the ocean height rises, a hydrodynamic pressure gradient across the subglacial cavity forces ocean water into the grounding zone, driving the inland migration of the grounding line. This process is analogous to a fluid-driven elastic peeling, or fracturing, problem (Lister et al., 2013; Hewitt et al., 2018; Tsai & Gudmundsson, 2015).

In the small region close to the grounding line, the pressure is predominantly due to elastic flexure of the ice, leading to characteristic flexural waves. If the incoming tide drives the grounding line inwards at speed U, then from equation (4) the viscous drag balances the elastic pressure gradient over a lengthscale $x \sim (Bh_0^3/12\mu U)^{1/5}$. Peeling is driven by the curvature $\kappa = \frac{\partial^2 h}{\partial x^2}$ at the grounding line,

$$\kappa \sim h_0/x^2 = 1.35(12\mu U/B)^{2/5}/h_0^{1/5}, \tag{5}$$

where the constant prefactor is calculated by Lister et al. (2013). The curvature is proportional to the lag of the grounding-line position behind the equilibrium height (see supporting information), so a balance is reached in which the grounding line can rise at the same speed as the incoming tide, with a small lag of

$$\Delta H = 1.35(12\mu U/B)^{2/5}(B/\rho g)^{1/2}/h_0^{1/5}. \tag{6}$$

3.2 The receding ocean tide

As the tide recedes, the water at the grounding line does not all instantly drain, but is initially retained against gravity, trapped in the hydrological network. This ocean water can be retained in the subglacial environment for substantial periods of time, since the drainage speed is controlled by the effective resistance to flow through the hydrological network, and driven only by the small along-slope component of gravity. The ocean height drops over a much shorter timescale, leaving behind the trapped water (figure 2b).

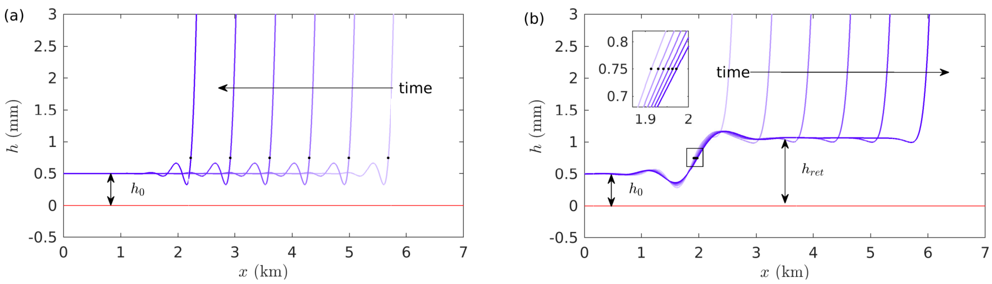

Figure 2. Results of a full numerical simulation for ocean height changing at constant speed of 2×10^{-4}ms^{-1} over a bedslope of $\theta = 10^{-3}$ with $h_0 = 0.5$mm, $B = 10^{16}$kgm^{2}s^{-2}. Colour gradient represents passage of time, profiles shown at 1 hour intervals. Black dots show the position of the grounding line. (a) As the ocean height rises, the grounding line migrates upwards at the same speed. At the grounding line, we observe flexural waves ahead of the peeling front. (b) As the ocean height falls, the majority of the water is able to drain out, but close to the grounding line, we find that a thin film of water is retained. The top-most extent of the film begins to slowly drain in a manner governed by equation (8) - see inset.

The effective depth of this volume of retained subglacial water can be determined from a balance in equation (4) between the drag resisting water flow out of the subglacial environment, and the elastic stresses forcing water out. This elastic mechanism is analogous to the process by which surface tension keeps surfaces wet even after they are withdrawn from a fluid. The elastic stresses are proportional to h_{ret}/x^3, and have magnitude $(\rho g/B)^{1/2}$. The flexural wavelength during drainage, $x \sim (Bh_{ret}^3/12\mu U)^{1/5}$, now also depends on the retained layer height. Combining these balances, we find that

$$h_{ret} = 5.12\frac{(\mu U)^{3/4}}{B^{1/8}(\rho g)^{5/8}\theta^{5/4}}, \tag{7}$$

with the constant prefactor found by Warburton et al. (2020). For tidal values of these parameters, h_{ret} is much larger than h_0. This implies that the background hydrological system of the grounding zone is overwhelmed by the additional ocean water, and this deposited fluid forms a much deeper layer between the ice and bed. This water-saturated area lubricates the contact between the ice and the bed, lowering the basal traction over this area of the grounding zone, even though the majority of the water has been evacuated.

While the tide retreats relatively rapidly, the retained water layer drains slowly under gravity, driven by hydrostatic pressure gradients. The fluid layer both thins (driven by gradients in h), and drains downslope (driven by the bedslope θ) and hence from equation (4) drainage is approximately governed by

$$\frac{\partial h}{\partial t} = \frac{\partial}{\partial x}\left[\frac{\rho g h_0^3}{12\mu}\left(\frac{\partial h}{\partial x} - \frac{3h\theta}{h_0}\right)\right] + O(h^2). \tag{8}$$

From equation (8), we see that at early times the drainage is mostly due to a thinning of the top-most extent of the layer, such that the distance the drained region migrates away from the high tide position is given by $x \sim \sqrt{\rho g h_0^3 t/\mu}$. At later times, the downslope drainage of the whole layer becomes the dominant mechanism, at constant speed $\rho g h_0^2\theta/4\mu$. In both regimes, the speed of drainage is limited by the effective permeability of the hydrological network, parametrised by h_0. If the permeability is large, the top of the fluid layer drains as quickly as it is deposited by the retreating tide. If the permeability is small, there is negligible drainage, and the ocean water deposited at high tide remains trapped over the tidal cycle.

From this continuous model for the evolution of h we can define a reduced model for the motion of the grounding line over the tidal cycle. The grounding-line position as defined here represents the position downstream of which a significant volume of water is retained between the ice and the bed, lubricating the contact such that the till exerts very little basal drag on the flow of the ice. Rosier & Gudmundsson (2020) highlight the sensitive role that variations in drag in the grounding zone play in setting the velocity response of ice shelves. In this way, modulations of horizontal ice velocity can be understood through the modulation of this position of decreased contact.

3.3 Grounding-line migration over the tidal cycle

We now consider the impact of multiple daily tidal cycles on the hydrology at the grounding zone, using as an illustrative example a far-field ocean height of

$$H_o(t) = A_M \sin(\omega_M t) + A_S \sin(\omega_S t). \tag{9}$$

This simplified forcing, with one lunar (M) and one solar (S) component, provides the interference between the two frequencies that produces a fortnightly amplitude variation at the M_{sf} frequency. Given the asymmetry between upslope and downslope grounding-line dynamics, we anticipate that the grounding zone acts as a non-linear filter on the ocean height, generating a response in the subglacial hydrological system at this 'beat' frequency.

Over the timescale of multiple tidal cycles, ice behaves visco-elastically. On the timescale of a single tidal cycle, the viscous behaviour appears as a small lag in the elastic response (Walker et al., 2013) or a weak modification to the bending stiffness (Reeh et al., 2003), so a purely elastic description effectively captures the daily dynamics. Over the longer fortnightly timescale, the ice acts passively as a boundary condition to the subglacial flow, and the rheology of the ice does not appear in the expression for the drainage speed (equation 8). Thus viscous flow of the ice is expected to have minimal impact on the asymmetry described here, which is set up by the short timescale elastic dynamics.

The grounding line moves upslope with the speed of the rising tide $U_{rise} \sim A\omega/\theta$, where $A = A_M + A_S$ is the maximum tidal amplitude, but as the tide retreats, the drainage speed is independent of the changes in ocean height, and is instead limited by the properties of the subglacial environment through equation (8) to

$$U_{receed} \sim \max\left(\sqrt{\frac{\rho g h_0^3 \omega}{\mu}}, \frac{\rho g h_0^2 \theta}{\mu}\right). \tag{10}$$

This fast upward motion, followed by a slower downwards retreat, leads to a grounding-line position that tracks the height of the high tide as it varies over the fortnightly cycle, smoothing out the daily tidal motion. We arrive at a reduced model for grounding-line migration governed only by the shape of the tidal forcing, and the ratio between downslope and upslope speeds,

$$r_{vel} = \max\left(\sqrt{\frac{\rho g h_0^3 \theta^2}{A^2 \mu \omega}}, \frac{\rho g h_0^2 \theta^2}{A \mu \omega}\right). \tag{11}$$

As these two parameter groupings have different dependence on h_0, we can separate out the uncertainty in h_0 from the uncertainty in the other parameters, transforming variables to the phase diagram shown in figure 3. This reduced system relies on just these two ratios and is computationally much simpler than solving the full model, so the grounding-line response can be easily calculated (see supporting material). This simple parameterisation of grounding-line motion could be implemented as a boundary condition in a larger scale ice sheet model, as demonstrated by Rosier & Gudmundsson (2020).

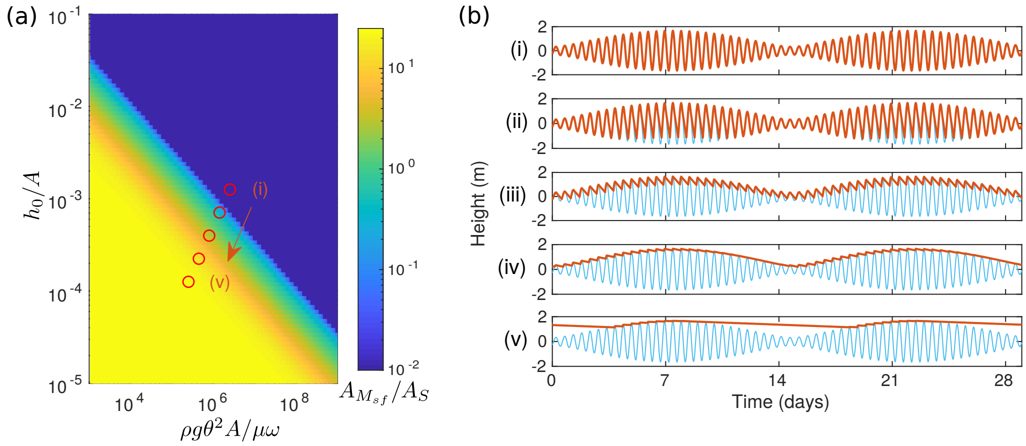

Figure 3. (a) Phase diagram showing the relative amplitudes of the 14-day ($A_{M_{sf}}$) to 12-hour (A_S) components present in the grounding-line position, as a function of dimensionless downslope gravity $\rho g \theta^2 A/\mu\omega$ and till permeability h_0/A. (Reduced model, forced by two sinusoidal frequencies with $\omega_M/\omega_S = 12.42/12$ and $A_M/A_S = 1.5$.) The points marked with open circles are shown in (b): Blue, tidal height, and red, grounding-line height. For very low permeability, the grounding line is pinned at the point of highest tide. As permeability increases, the high frequency components are more weakly filtered.

As a quantitative measure for the degree of non-linearity in our simple tidal example, we use the ratio of amplitudes between the 14-day and the 12-hour frequencies, $A_{M_{sf}}/A_S$, in the Fourier spectrum of the grounding-line motion (for a more complete tidal model, one could adapt this measure to use the amplitudes of the dominant frequencies). This description clearly distinguishes between cases where the lower frequency is not generated, cases where both frequencies are present in the motion, and cases where the response is entirely at the 14-day frequency (figure 3). This measure is a function of model output alone, so can be directly applied to observations of other quantities for comparison.

If drainage is fast, with barely any drag exerted by the hydrological system, then the grounding line can move up and down freely with the daily tides, producing a predominantly diurnal response (figure 3i). This occurs if $r_{vel} > 1$, which is possible for small-amplitude tides over steep bedslopes. For smaller permeability of the subglacial environment, the magnitude of the daily motion is limited by the distance that the grounding line can migrate in one day (figure 3ii). This response is consistent with the observations from the Bindschadler Ice Stream (Anandakrishnan et al., 2003) which show that the amplitude of the flow fluctuations does not vary with the amplitude of the ocean tides. For even smaller subglacial permeabilities, the grounding line acts as a filter on the tidal signal, moving with the frequency of the amplitude envelope, generating a more dominant fortnightly component to the response (figure 3iii-iv). This ranges between a small amplitude variation similar to the response observed at Beardmore Glacier (Marsh et al., 2013), to the predominantly fortnightly variations seen in observations of Rutford Ice Stream (Minchew et al., 2017). If the drainage is slow enough, the grounding line becomes essentially fixed at the high tide position, disconnecting the response of the grounded ice from the ocean tides (figure 3v). Many glaciers that exhibit no tidal response could plausibly fall into this category.

We may apply our reduced model of grounding-line motion to the tidal model for ocean height described by Padman et al. (2002), at both the Rutford Ice Stream (flowing into the Ronne Ice Shelf) and Beardmore Glacier (flowing into the Ross). Values for

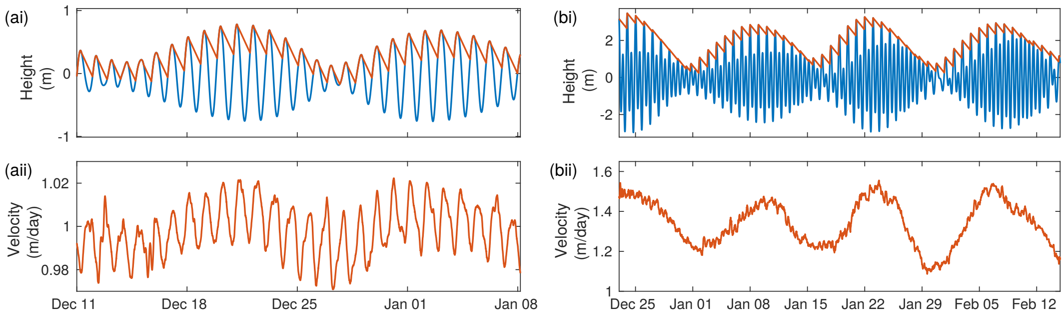

Figure 4. (i) Results of the reduced model for grounding line position with $h_0 = 10^{-4}$m applied to the tides at the grounding lines of (ai) Beardmore Glacier, and (bi) Rutford Ice Stream. The difference in grounding-line response can be attributed to the differing tidal amplitudes. CATS2008 tidal model described in Padman et al. (2002) used to force both. (ii) 3-day rolling average of ice horizontal surface velocity from the same locations and dates. Beardmore data (aii) from Marsh et al. (2013), (bii) Rutford data from Gudmundsson (2006).

tidal amplitude $A \sim 3$m and frequency $\omega \sim 10^{-5}\text{s}^{-1}$ are taken from Padman et al. (2002), and ρ, g, and μ are well documented for water. At the grounding line of both Rutford and Beardmore, the isostatic gradient is of order $\theta - \frac{\rho_i}{\rho}\frac{dD}{dx} \sim 10^{-2}$ (Morlighem et al., 2020), where $\rho_i \approx 0.9\rho$ is the density of ice. From the phase diagram in figure 3a we estimate that for Rutford, where $\rho g \theta^2 A/\mu\omega \sim 10^8$, we require $h_0/A \sim 10^{-4.5}$ for strong filtering. By contrast, since tidal amplitudes are lower over the Ross Ice Shelf, that same hydraulic system would lead to much weaker filtration (figure 4), consistent with the primarily diurnal response of the glaciers feeding the Ross. This value of h_0 represents a permeability thickness of 10^{-12}m^3, consistent with estimates of till permeability of $10^{-11} - 10^{-19}\text{m}^2$ for tills of thickness $10^{-2} - 10$m (Fischer et al., 1998).

4 Conclusions

We have presented a mathematical description of the migration of ocean water through the subglacial cavity at the grounding zones of ice sheets. We have shown how an asymmetry in the physics governing incoming and outgoing migration leads to a non-linear response to the tidal forcing that is able to generate new frequencies at the grounding line itself. The model reconciles observations of ice stream velocity variations from across Antarctica and Greenland, and provides a new constraint on the effective permeability of the subglacial environment at these locations.

The model predicts that a significant amount of ocean water is retained in the subglacial environment. An outstanding question remains to determine the processes whereby this non-linear response of the subglacial water pressure is transmitted upstream of the grounding zone through the till, and to what extent this impacts on till rheology and glacial sliding. The tidal flushing of ocean water in regions conventionally understood to be grounded may also play a role in increased glacial melting as the oceans warm.

Acknowledgments

K.L.P.W. is supported by the Natural Environment Research Council (grant no. NE/L002507/1). No new data were used in this manuscript; the CATS2008 tidal model is described in Padman et al. (2002), the Rutford GPS data in Gudmundsson (2006). We thank O. Marsh for providing the processed Beardmore GPS data from Marsh et al. (2013).

References

Anandakrishnan, S., Voigt, D. E., Alley, R. B., & King, M. A. (2003). Ice stream D flow speed is strongly modulated by the tide beneath the Ross Ice Shelf. *Geophys. Res. Lett.*, *30*(7). doi: 10.1029/2002GL016329

Bamber, J. L., Gomez-Dans, J. L., & Griggs, J. A. (2009). A new 1 km digital elevation model of the Antarctic derived from combined satellite radar and laser data – Part 1: Data and methods. *Cryosphere*, *3*(1), 101–111. doi: 10.5194/tc-3-101-2009

Bamber, J. L., & Rivera, A. (2007). A review of remote sensing methods for glacier mass balance determination. *Global and Planetary Change*, *59*(1), 138–148.

Bindschadler, R. A., Vornberger, P. L., King, M. A., & Padman, L. (2003). Tidally driven stick-slip motion in the mouth of Whillans Ice Stream, Antarctica. *Ann. Glaciol.*, *36*, 263-272. doi: 10.3189/172756403781816284

Bougamont, M., Christoffersen, P., Hubbard, A. L., Fitzpatrick, A. A., Doyle, S. H., & Carter, S. P. (2014). Sensitive response of the Greenland Ice Sheet to surface melt drainage over a soft bed. *Nat. Commun.*, *5*(1), 5052. doi: https://doi.org/10.1038/ncomms6052

Brunt, K. M., Fricker, H. A., Padman, L., Scambos, T. A., & O'Neel, S. (2010). Mapping the grounding zone of the Ross Ice Shelf, Antarctica, using ICESat laser altimetry. *Ann. Glaciol.*, *51*(55), 7179. doi: 10.3189/172756410791392790

Fischer, U. H., Iverson, N. R., Hanson, B., LeB. Hooke, R., & Jansson, P. (1998). Estimation of hydraulic properties of subglacial till from ploughmeter measurements. *J. Glaciol.*, *44*(148), 517522. doi: 10.3189/S0022143000002033

Gillet-Chaulet, F., & Durand, G. (2010). Ice–sheet advance in Antarctica. *Nature*, *467*(7317), 794–795. doi: https://doi.org/10.1038/467794a

Gudmundsson, G. H. (2006). Fortnightly variations in the flow velocity of Rutford Ice Stream, West Antarctica. *Nature*, *444*, 1063–1064. doi: 10.1038/nature05430

Gudmundsson, G. H. (2013). Ice-shelf buttressing and the stability of marine ice sheets. *Cryosphere*, *7*(2), 647–655. doi: 10.5194/tc-7-647-2013

Hewitt, D. R., Chini, G. P., & Neufeld, J. A. (2018). The influence of a poroelastic till on rapid subglacial flooding and cavity formation. *J. Fluid Mech.*, *855*, 11701207. doi: 10.1017/jfm.2018.624

Holdsworth, G. (1969). Flexure of a floating ice tongue. *J. Glaciol.*, *8*(54), 385397. doi: 10.3189/S0022143000026976

Iverson, N. R. (2010). Shear resistance and continuity of subglacial till: hydrology rules. *J. Glaciol.*, *56*(200), 11041114. doi: 10.3189/002214311796406220

Jenkins, A., Dutrieux, P., Jacobs, S. S., McPhail, S. D., Perrett, J. R., Webb, A. T., & White, D. (2010). Observations beneath Pine Island Glacier in West Antarctica and implications for its retreat. *Nat. Geosci.*, *3*(7), 468–472.

Larour, E., Rignot, E., Joughin, I., & Aubry, D. (2005). Rheology of the Ronne Ice Shelf, Antarctica, inferred from satellite radar interferometry data using an inverse control method. *Geophys. Res. Lett.*, *32*(5). doi: 10.1029/2004GL021693

Le Brocq, A., Payne, A., Siegert, M., & Alley, R. (2009). A subglacial waterflow model for West Antarctica. *J. Glaciol.*, *55*(193), 879888. doi: 10.3189/002214309790152564

Lister, J. R., Peng, G. G., & Neufeld, J. A. (2013). Viscous control of peeling an elastic sheet by bending and pulling. *Phys. Rev. Lett.*, *111*, 154501. doi: 10.1103/PhysRevLett.111.154501

Marsh, O. J., Rack, W., Floricioiu, D., Golledge, N. R., & Lawson, W. (2013). Tidally induced velocity variations of the Beardmore Glacier, Antarctica, and their representation in satellite measurements of ice velocity. *Cryosphere*, *7*(5), 1375–1384. doi: 10.5194/tc-7-1375-2013

Minchew, B. M., Simons, M., Riel, B., & Milillo, P. (2017). Tidally induced variations in vertical and horizontal motion on Rutford Ice Stream, West Antarctica, inferred from remotely sensed observations. *J. Geophys. Res. Earth Surface*, *122*(1), 167-190. doi: 10.1002/2016JF003971

Morlighem, M., Rignot, E., Binder, T., Blankenship, D., Drews, R., Eagles, G., ... Young, D. A. (2020). Deep glacial troughs and stabilizing ridges unveiled beneath the margins of the Antarctic ice sheet. *Nat. Geosci.*, *13*(2), 132–137. doi: https://doi.org/10.1038/s41561-019-0510-8

Padman, L., Fricker, H. A., Coleman, R., Howard, S., & Erofeeva, L. (2002). A new tide model for the Antarctic ice shelves and seas. *Ann. Glaciol.*, *34*, 247254. doi: 10.3189/172756402781817752

Padman, L., Siegfried, M. R., & Fricker, H. A. (2018). Ocean tide influences on the Antarctic and Greenland ice sheets. *Rev. of Geophys.*, *56*(1), 142-184. doi: 10.1002/2016RG000546

Reeh, N., Christensen, E. L., Mayer, C., & Olesen, O. B. (2003). Tidal bending of glaciers: a linear viscoelastic approach. *Annals of Glaciology*, *37*, 8389. doi: 10.3189/172756403781815663

Rignot, E., Mouginot, J., & Scheuchl, B. (2011). Antarctic grounding line mapping from differential satellite radar interferometry. *Geophys. Res. Lett.*, *38*(10). doi: 10.1029/2011GL047109

Rosier, S. H. R., & Gudmundsson, G. H. (2018). Tidal bending of ice shelves as a mechanism for large-scale temporal variations in ice flow. *Cryosphere*, *12*(5), 1699–1713. doi: 10.5194/tc-12-1699-2018

Rosier, S. H. R., & Gudmundsson, G. H. (2020). Exploring mechanisms responsible for tidal modulation in flow of the Filchner–Ronne Ice Shelf. *Cryosphere*, *14*(1), 17–37. doi: 10.5194/tc-14-17-2020

Rosier, S. H. R., Gudmundsson, G. H., & Green, J. A. M. (2015). Temporal variations in the flow of a large Antarctic ice stream controlled by tidally induced changes in the subglacial water system. *Cryosphere*, *9*(4), 1649–1661. doi: 10.5194/tc-9-1649-2015

Sayag, R., & Worster, M. G. (2011). Elastic response of a grounded ice sheet coupled to a floating ice shelf. *Phys. Rev. E*, *84*, 036111.

Sayag, R., & Worster, M. G. (2013). Elastic dynamics and tidal migration of grounding lines modify subglacial lubrication and melting. *Geophys. Res. Lett.*, *40*(22), 5877-5881. doi: 10.1002/2013GL057942

Schoof, C. (2007). Ice sheet grounding line dynamics: Steady states, stability, and hysteresis. *J. Geophys. Res. Earth Surface*, *112*(F3). doi: 10.1029/2006JF000664

Shepherd, A., Ivins, E. R., A, G., Barletta, V. R., Bentley, M. J., Bettadpur, S., ... Zwally, H. J. (2012). A reconciled estimate of ice-sheet mass balance. *Science*, *338*(6111), 1183–1189. doi: 10.1126/science.1228102

Tsai, V. C., & Gudmundsson, G. H. (2015). An improved model for tidally modulated grounding-line migration. *J. Glaciol.*, *61*(226), 216222. doi: 10.3189/2015JoG14J152

Tulaczyk, S., Kamb, W. B., & Engelhardt, H. F. (2000). Basal mechanics of Ice Stream B, West Antarctica: 1. Till mechanics. *J. Geophys. Res. Solid Earth*, *105*(B1), 463-481. doi: 10.1029/1999JB900329

Vaughan, D. G. (1995). Tidal flexure at ice shelf margins. *J. Geophys. Res. Solid Earth*, *100*(B4), 6213-6224. doi: 10.1029/94JB02467

Walker, R. T., Parizek, B. R., Alley, R. B., Anandakrishnan, S., Riverman, K. L., & Christianson, K. (2013). Ice-shelf tidal flexure and subglacial pressure variations. *Earth Planet. Sci. Lett.*, *361*, 422–428.

Warburton, K. L. P., Hewitt, D. R., & Neufeld, J. A. (2020). The elastic Landau-Levich problem on a slope. *J. Fluid Mech.*, *883*, A40. doi: 10.1017/jfm.2019.910